Spectroscopy of ^{13,14}B via the one-neutron knockout reaction

V. Guimarães and J. J. Kolata
Physics Department, University of Notre Dame, Notre Dame, Indiana 46556

D. Bazin, B. Blank, B. A. Brown, T. Glasmacher, P. G. Hansen, R. W. Ibbotson, D. Karnes, V. Maddalena, A. Navin, B. Pritychenko, and B. M. Sherrill
National Superconducting Cyclotron Laboratory, Michigan State University, East Lansing, Michigan 48824

D. P. Balamuth and J. E. Bush
Physics Department, University of Pennsylvania, Philadelphia, Pennsylvania 19104
(Received 27 January 2000; published 12 May 2000)

The single-nucleon knockout reactions ^{9}Be(^{14}B,^{13}B+γ)X and ^{197}Au(^{14}B,^{13}B+γ)X, at an incident energy of 60 MeV per nucleon, have been used to probe the structure of ^{14}B and of the core fragment ^{13}B. A dominant $2s$ configuration is deduced for the neutron in the ground state of ^{14}B. The longitudinal momentum distribution for this state is consistent with ''neutron halo'' structure. Spin assignments for ^{13}B excited states at 3.48 and 3.68 MeV are proposed based on the observed spectroscopic factors for one-neutron removal.

PACS number(s): 25.60.Gc, 21.10.Jx, 27.20.+n

I. INTRODUCTION

The structure and reactions of ''neutron-halo'' nuclei, weakly bound systems that display a very diffuse surface of nearly pure neutron matter at densities far below that of normal nuclear matter, have recently been subjects of intense study [1]. In a highly simplified picture, the longitudinal momentum distribution of fragments from the breakup of a loosely bound projectile directly reflects the internal momentum distribution of the valence nucleon and hence the square of the Fourier transform of its wave function. Thus, halo formation in such loosely bound nuclei can be investigated by measuring the momentum distribution of the fragment from a breakup reaction. The wide spatial dispersion characteristic of a halo neutron translates into a narrow momentum distribution. In this model, one treats the core of the nucleus as an inert spectator to the breakup process. While early experiments were based on the assumption that the measured momentum distribution represented a single reaction channel, it has recently become possible to go beyond this naive approach by measuring γ radiation from the decay of excited states of the core in coincidence with the breakup fragments [2]. This technique provides a further benefit in that partial cross sections for the excitation of different final states of the core can be measured, together with the longitudinal momentum distributions associated with inert and ''active'' cores. This allows for spectroscopic investigation of both the core nucleus and the valence nucleon(s). The method, originally developed in a search for proton halo nuclei [2], has also been applied to the neutron case [3,4].

Among the candidates for neutron halo formation, the ^{14}B nucleus is of particular interest as the lowest-mass bound system amongst the $N=9$ isotones. The well-known halo nuclei ^{11}Be, ^{11}Li, ^{14}Be, ^{17}B, and ^{19}C occupy a similar position for $N=7$, $N=8$, $N=10$, $N=12$, and $N=13$, respectively (see Refs. [5–7], and references therein, for a discussion of ^{19}C structure). Moreover, ^{14}B is an odd-odd nucleus and thus different from any other neutron-halo system observed to date. In the first attempt to probe the structure of ^{14}B, Bazin *et al.* [8] reported a broadening of the longitudinal momentum distribution when compared with the shape expected from theoretical predictions, and suggested that this difference might be due to a strong contribution from core excitation. As a result, they were unable to draw any firm conclusion about halo formation in this nucleus. In order to investigate the structure of ^{14}B, and to determine the role that the core plays in the dissociation reaction, the momentum distributions of ^{13}B fragments corresponding to removal of neutrons from different orbitals in ^{14}B were measured using the technique described in Ref. [2]. The contribution from core excitation was isolated by measuring the momentum distribution of excited ^{13}B fragments in coincidence with γ rays from their decay.

This paper is divided into the following sections. The experimental setup and the procedure are described in Sec. II, while the experimental results and the analysis of the longitudinal momentum distributions is presented in Sec. III. Finally, a summary is given in Sec. IV.

II. EXPERIMENT

The experiment was performed at the National Superconducting Cyclotron Laboratory (NSCL) at Michigan State University. The ^{14}B radioactive secondary beam was produced by fragmentation of an 80 MeV per nucleon primary ^{18}O beam on a 790 mg/cm^2 Be target. The secondary ^{14}B beam, having an energy of 59.2 ± 0.3 MeV per nucleon, was then selected by the A1200 fragment separator [9] and transmitted to a target chamber where a neutron was removed during an interaction with a Be or Au target, leaving the ^{13}B core in its ground state or in an excited state. The γ rays from the decay of ^{13}B excited states were detected by an array of 38 cylindrical NaI (Tl) detectors [10] which completely surrounded the target. Recoiling ^{13}B core fragments were momentum analyzed using the S800 spectrograph [11]. The momentum acceptance of the spectrograph was 6% and

the angular acceptances were $\pm 3.5°$ and $\pm 5°$ in the dispersive and nondispersive directions, respectively. These acceptances resulted in an estimated 99% efficiency for detecting events corresponding to the ground-state momentum distribution, and 95% for the momentum distributions of the excited states, as determined from the observed shapes. This point is discussed further below. The spectrograph was operated in dispersion-matched mode, in which the intrinsic dispersion of the secondary beam (0.5%) is compensated by the last section of the spectrometer. The targets of Be and Au were 228 and 256 mg/cm^2 thick, respectively, chosen to produce an energy straggling of about the same magnitude as the resolution of the spectrograph. The overall resolution (including target thickness effects) was measured to be 9 MeV/c full width at half maximum (FWHM) in a direct-beam run with the target in place. This run also gave the normalization for the beam flux, determined to be 5×10^3 particles/s.

Time-of-flight information (over a distance of 70 m) combined with the energy loss and total energy signal obtained with a segmented ion chamber and a 5 cm thick plastic scintillator, respectively, were used to identify and measure the yields of the fragments in the focal plane of the spectrograph. Two x/y position-sensitive cathode-readout drift chambers in the focal plane were used to determine the momentum and angle information of the fragments.

III. EXPERIMENTAL RESULTS

A. Cross sections and spin assignments for ^{13}B

An energy spectrum of γ rays in coincidence with ^{13}B fragments is shown in Fig. 1. This spectrum has been transformed into the projectile rest frame using the position of the incident γ ray measured in the NaI array, which allows for Doppler correction on an event-by-event basis. The solid curve is a fit to the data obtained via Monte-Carlo simulation using the code GEANT [12]. The simulation took into account Doppler broadening, the distortion of the shapes caused by the back transformation to the projectile rest frame, and the calculated γ-ray detection efficiencies. Experimental efficiencies measured with calibrated radioactive sources agreed with the simulation to within 5% The background, which presumably results from a combination of breakup reactions leaving the target in an excited state and secondary interactions of neutrons with the detector and surrounding materials, was parametrized by a simple exponential dependence. Taking into account the 3.48, 3.68, and 4.13 MeV transitions in ^{13}B, the fit to the experimental spectrum is excellent (the χ^2 per degree of freedom N is 1.08). The choice of these particular γ-ray transitions is discussed below. Eliminating the 4.13 MeV γ ray from the fit causes χ^2/N to increase to 1.10 for 170 degrees of freedom, which is marginally significant. This indicates that all the important transitions were accounted for and that there are no other significant γ rays between 1.5 and 3.5 MeV or above 4.2 MeV.

The level scheme of ^{13}B [13] is presented in Fig. 2. The ground state has $J^\pi=\frac{3}{2}^-$, resulting from a $[1p_{3/2}]^{-1}$ proton configuration. Below 4.5 MeV, three negative parity and two positive parity excited states have been identified. Although the energies and parities of these states are well established

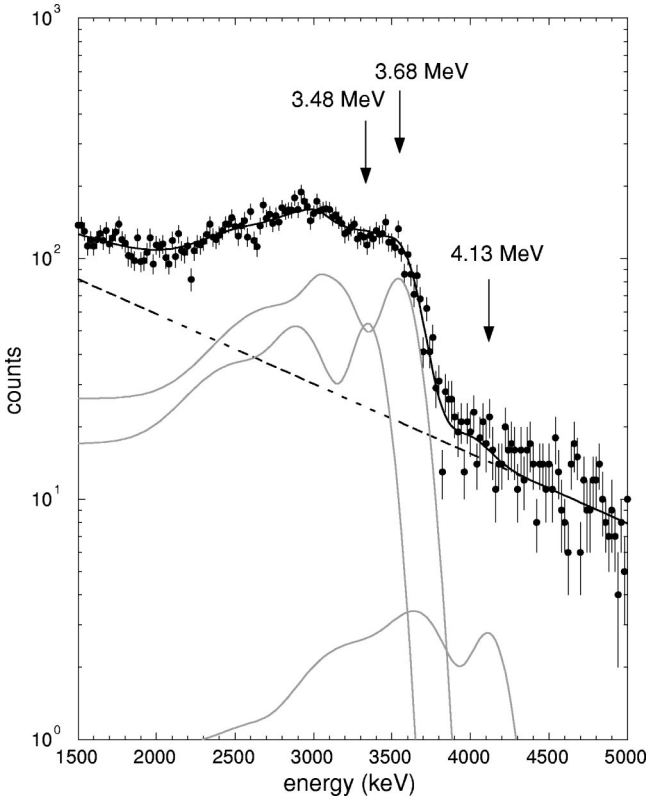

FIG. 1. Doppler corrected energy spectrum of the γ rays measured in coincidence with a ^{13}B fragment in the NaI array. The solid line is the fit to the experimental data. The fit corresponds to an independent normalization of the simulated response functions for each individual γ ray, indicated in the figure by the gray curves. The background is parametrized by an exponential dependence.

from particle-transfer reaction studies, very little is known about their spins. Based on the γ-ray spectrum of Fig. 1, we are interested in the group of states between 3.48 and 4.13 MeV. The limited energy resolution of NaI (Tl) detectors does not allow for separation of the two close-lying doublets in this spectrum, so it is necessary to invoke arguments from theoretical considerations to resolve the ambiguity. Future experiments with high-resolution Ge detectors will allow for a test of these arguments.

In the simplest model, the $J^\pi=2^-$ ground state of ^{14}B results from the coupling of a $2s1d$-shell neutron to the ^{13}B ground state. Then, the neutron removal from ^{14}B could proceed by the removal of the sd-shell neutron to leave ^{13}B in its ground state, by removal of a neutron from the $1p_{1/2}$ orbital leaving ^{13}B in an excited state with $J^\pi=3/2^+,5/2^+$, or by removal of a neutron from the $1p_{3/2}$ orbital leaving ^{13}B in a more highly excited state with $J^\pi=1/2^+,3/2^+,5/2^+$, or $7/2^+$.

This simple model is confirmed by shell-model calculations in the $1p$-$2s1d$ model space with the WBT and WBP residual interactions [15]. Calculations were carried out for the ^{14}B ground state with a $(1p)^{-3}(sd)^1$ configuration (relative to a closed shell for ^{16}O), and for the ^{13}B spectrum with $(1p)^{-3}(2s1d)^0$, $(1p)^{-4}(2s1d)^1$, and $(1p)^{-5}(2s1d)^2$ configurations. (The total number of eigenstates are 5, 299, and

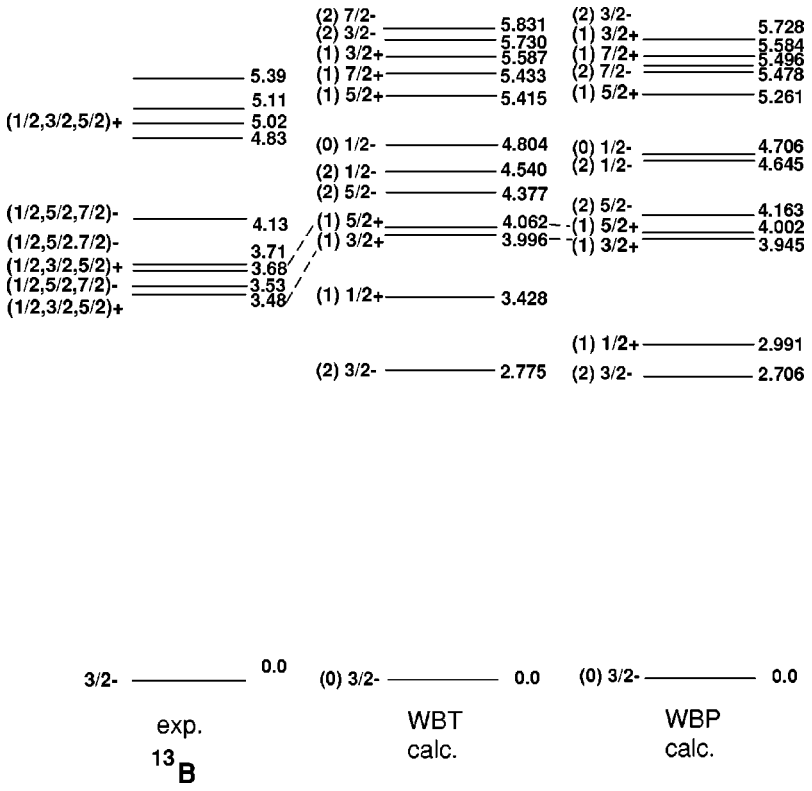

FIG. 2. The level scheme of ^{13}B. The experimental data are from Ref. [13] (and references therein), and the theoretical predictions are from a shell model calculation. The values given in parentheses are the numbers of neutrons (ΔN) excited to the *sd* shell. The dashed lines correspond to the assignments discussed in the text.

2973, respectively.) The low-lying energy levels obtained for these configurations, labeled by $\Delta N=0$, 1, and 2, respectively, are shown in Fig. 2. (Mixing between the $\Delta N=0$ and $\Delta N=2$ configurations will be discussed below.) The spectroscopic factors for the WBT interaction are given in Table I (the spectroscopic factors obtained with WBP are similar to those of WBT). The higher levels, which are reached by predominantly $1p_{3/2}$ removal, lie above the neutron decay threshold of 4.9 MeV. The spectroscopic factors leading to the $\Delta N=2$ configurations are zero with our configuration assumptions. All of the $\Delta N=0$, 1, and 2 configurations are allowed in the ^{11}B$(t,p)^{13}$B reaction which has been previously used to identify the ^{13}B states [16].

TABLE I. Partial cross sections in mb for each of the final states populated in ^{13}B. The spin assignments for each level (third column) are discussed in the text. The fourth and fifth columns are the orbital angular momentum of the valence neutron and the corresponding spectroscopic factor, respectively. The next three columns give the partial cross sections for stripping and diffractive breakup in the eikonal model of Ref. [17], and the theoretical value for the cross section which is the sum of the two components multiplied by the corresponding spectroscopic factor. The experimental value is given in the last column.

$E^{\rm exp}$ (MeV)	$E^{\rm theo}$ (MeV)	J^π	l	S	$\sigma_{\rm SP}^{\rm strip}$	$\sigma_{\rm SP}^{\rm diff}$	$\sigma^{\rm theo}$	$\sigma^{\rm exp}$
0.00	0.00	$\frac{3}{2}^-$	0	0.662	82.4	53.9	90.2	113 (15) [a]
			2	0.306	35.0	16.5	15.8	14 (3) [a]
	3.43	$\frac{1}{2}^+$	1	0.092	24.1	9.7	3.1	
3.48	4.00	$\frac{3}{2}^+$	1	0.407	24.1	9.7	14.0	18 (3)
3.68	4.06	$\frac{5}{2}^+$	1	0.886	23.5	9.4	29.2	30 (5)
4.13								1.2 (1.2)
	4.80	$\frac{1}{2}^-$	2	0.0005	22.3	8.0	0.014	

[a]Cross section obtained by deconvolution of the $l=0$ and $l=2$ contributions to the longitudinal momentum distribution.

In principle, the $\Delta N=0$ and $\Delta N=2$ configurations can be mixed, which could give some spectroscopic strength leading to negative parity states around 4 MeV in excitation. It is well known that the mixing of $\Delta N=2$ into $\Delta N=0$ is very large, about 30% [14]. However, the mixing is coming mostly from high-lying (10–20 MeV) $\Delta N=2$ configurations through the strong $(\lambda,\mu)=(2,0)$ component of the interaction. The mixing of the low-lying $\Delta N=2$ configuration which appear in the spectrum of Fig. 1 is small. It is difficult to carry out a mixed calculation because $\Delta N=4$ configurations would also be needed to give the correct relative energies of the $\Delta N=0$ and $\Delta N=2$ configurations, and this is beyond the scope of the present calculations. We estimated the mixing with the ''shift'' method [14] of lowering the diagonal energy of the $\Delta N=2$ configurations to account for absence of $\Delta N=4$. The resulting wave functions for the ^{13}B and ^{14}B ground states have about 30% $\Delta N=2$, but the spectroscopic factors to the negative parity states in the region of 4 MeV in ^{13}B are small, on the order of 0.02 or less, for the reason discussed above. These states are therefore neglected in the discussion below. However, it should be noted that the core-excited momentum distribution (see below) is in good agreement with expectations for removal of a $1p_{1/2}$ neutron from the $J^\pi=2^-$ ground state of ^{14}B, which populates only positive-parity states. The *d*-state contamination, leading to

negative parity states, must be quite small as indicated by the theoretical calculation.

Partial cross sections obtained from the absolute γ-ray intensities corrected by the computed efficiencies and the spectrometer acceptance are presented in Table I. The overall error in these cross sections are of the order of 18%, due mainly to systematic errors in the fit to the experimental γ-ray spectrum, and to the uncertainties in the number of particles in the beam (12%) and the target thickness (5%).

The calculated cross section for each final state of the core fragment in a one-nucleon knockout reaction is given by

$$\sigma(n)=\sum_j C^2S(j,n)\sigma_{sp}(j,B_n), \tag{1}$$

where $C^2S(j,n)$ is the computed spectroscopic factor for the removed nucleon with respect to a given core state and $\sigma_{sp}(j,B_n)$ is the reaction cross section for the removal of a nucleon from a single-particle state with total angular momentum j. B_n is the sum of the separation energy and excitation energy of the state n. The single-particle cross sections were calculated by Tostevin [17] in a eikonal model assuming that there are two reaction mechanisms involved in the knockout reaction: (i) nucleon stripping in which the halo nucleon interacts strongly with the target and leaves the beam and (ii) diffraction dissociation in which the nucleon moves forward with essentially the beam velocity but away from the core.

The calculated cross sections for the states below 4.5 MeV are given in Table I. The best agreement with experiment is achieved with the spin assignments shown there. It should be noted that the evidence for the existence of the 4.13 MeV transition in the experimental γ-ray spectrum is marginal. Furthermore, the calculated strength for this transition (Table I) does not take into account the configuration mixing discussed above. Overall, it appears that the combination of the theoretical spectroscopic factors and computed single-particle cross sections does a remarkable job of reproducing the experimental yields.

B. Momentum distributions

The momentum vector of the fragment at the target position after the reaction was reconstructed using the known magnetic fields and the positions and angles at the focal plane, and the ion-optics code COSY [18]. The momentum components transverse to the beam direction are sensitive to the reaction mechanism, while the longitudinal momentum component is relatively independent of the details of the reaction mechanism as discussed by Orr *et al.* [19]. The longitudinal momentum distribution is obtained as the projection of the total momentum in the direction parallel to the beam. From the coincident γ-ray data, it is possible to generate the distribution for the case when ^{13}B is left in its ground state, by subtracting the contribution from the excited states from the singles spectrum after correcting for the γ-ray detection efficiencies. The result of this subtraction process is presented in Fig. 3(a) and corresponds to the removal of a single neutron from the sd shell in ^{14}B due to a reaction with a ^{9}Be target. Figure 3(b) shows the longitudinal momentum distribution for the core-excited states, which is considerably broader.

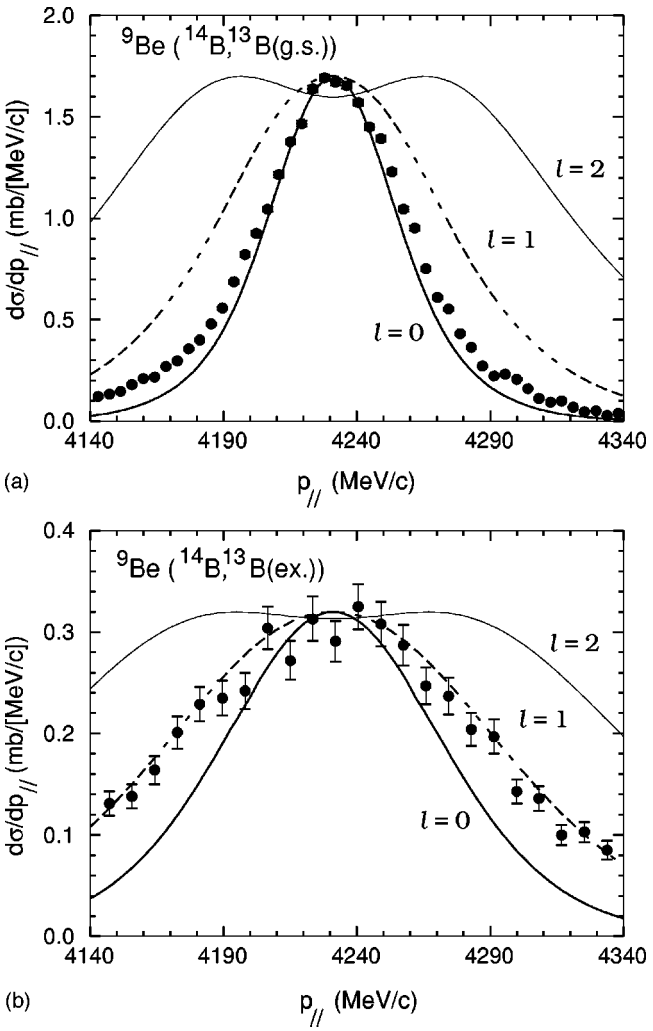

FIG. 3. The longitudinal momentum distribution of the ^{13}B core fragment, in the laboratory frame, from one-neutron knockout reaction from ^{14}B incident on a ^{9}Be target. (a) Longitudinal momentum distribution corresponding to the ^{13}B core in its ground state. (b) The same, but for ^{13}B core-excited states. The error bars indicate only the statistical uncertainties. The thick solid, dashed, and thin solid curves correspond to the momentum distributions calculated in the eikonal model for the removal of a neutron in an s, p, or d orbital, respectively.

A more precise comparison can be made through the use of the reaction theory. Calculated longitudinal momentum distributions, also shown in Fig. 3, were determined within the framework of the eikonal model following the procedure of Ref. [20]. Since the dissociation products are formed at an impact parameter greater than $b_{\min}=R_C+R_n$ (where R_C and R_n are the energy-dependent radii for the core and valence nucleon, usually chosen to reproduce the measured interaction cross section) the black disc approximation can be used. The cross section is then expressed in terms of the impact parameter as the one-dimensional Wigner transform of the wave function after the reaction, where the wave function

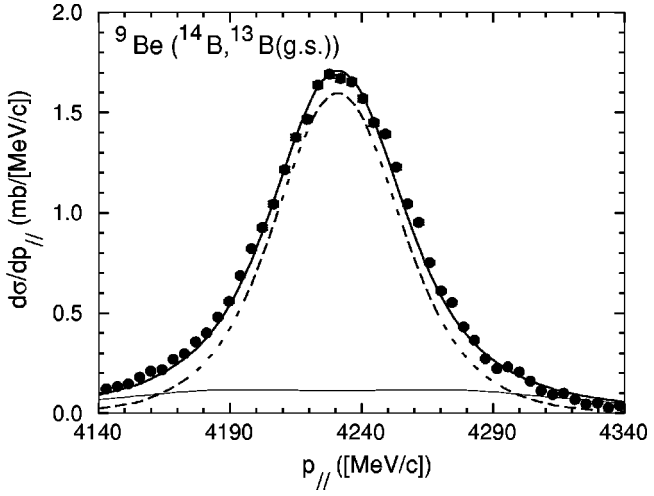

FIG. 4. The longitudinal momentum distribution with the ^{13}B core fragment in its ground state. The thick solid line is the result of a fit with a linear combination of the $l=0$ and $l=2$ shapes from the eikonal model. The dashed curve and thin solid curve are the individual contributions for $l=0$ and $l=2$, respectively.

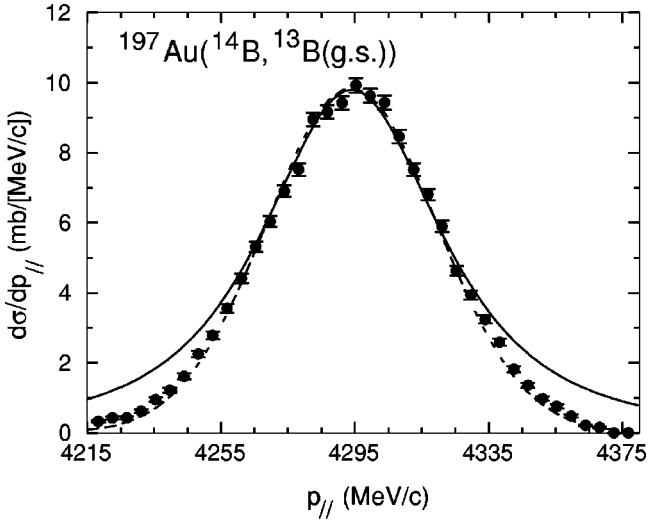

FIG. 5. The longitudinal momentum distribution with the ^{13}B core fragment in its ground state for the Coulomb breakup of ^{14}B on a ^{197}Au target. The dashed curve is a Gaussian fit having a width of 60 ± 3 MeV/c FWHM. The solid curve is the result of a calculation using a Yukawa potential with finite-size corrections [21].

profile is unity outside of a cutoff radius and zero inside. The momentum distribution corresponding to the ^{13}B core in its ground state, shown in Fig. 3(a), agrees reasonably well with the $l=0$ curve of the eikonal model calculation, which represents the removal of an *s*-wave valence neutron from the *sd* shell in ^{14}B. Similar results have been obtained for ^{11}Be [3] and ^{15}C [4]. The width obtained for the distribution is 55 ± 2 MeV/c FWHM, after correcting for the 9 MeV/c experimental momentum resolution. This width results from a Lorentzian fit to the experimental data and is in excellent agreement with the value of 56 MeV/c FWHM displayed by the theoretical $l=0$ curve in the laboratory system. The disagreement in the tails of the distribution suggests that there may be a contribution from the $l=2$ distribution and possibly other effects due to the acceptance of the spectrometer, approximations in the reaction model used to analyze the data, or unidentified contributions to the line shape [3].

Spectroscopic factors of 0.306 and 0.662, respectively, are obtained from the shell model calculation [15] for the removal of a valence neutron from the $1d_{5/2}$ and $2s_{1/2}$ states in ^{14}B, which indicates that a non-negligible $l=2$ admixture is expected. Individual cross sections for both configurations have been derived by fitting the experimental distribution with a linear combination of $l=0$ and $l=2$ shapes. The best fit, shown in Fig. 4, implies that the removal of a valence neutron from the $2s_{1/2}$ ($1d_{5/2}$) orbital in the ^{14}B ground state accounts for $89\pm3\%$ ($11\pm3\%$) of the total yield. The agreement with cross sections derived from the eikonal model and the theoretical spectroscopic factors is very good (Table I), as is the quality of the fit to the experimental data shown in Fig. 4.

The core-excited longitudinal momentum distribution, shown in Fig. 3(b), was obtained from the γ-ray-coincident ^{13}B yield after subtracting a background distribution derived by gating on the exponential part of the γ-ray spectrum at high energy and normalizing to the extrapolated background under the peaks. The background computed in this way constituted 26% of the coincident data in the region of the three identified γ-ray transitions. The core-excited distribution has a shape that agrees well with that expected for $l=1$, confirming the expectation of the removal of a $1p_{1/2}$ neutron. The experimental width, obtained from a Lorentzian fit to the central part of the distribution, is 135 ± 15 MeV/c FWHM. The calculated width in the laboratory frame of the theoretical $l=1$ curve is 144 MeV/c. The distributions computed for *p* and *d* wave breakup are broader than the actual momentum acceptance of the spectrometer. A (small) correction to the integrated yield due to this limited acceptance has been applied to the experimental cross sections given in Table I.

C. Coulomb breakup

The longitudinal momentum distribution obtained in the one-neutron breakup reaction of ^{14}B on a ^{197}Au target is shown in Fig. 5. The γ-ray coincident yield has been subtracted using the same procedure as described in the previous section. In this case, the γ-ray spectrum was essentially equal to the exponential background distribution, and no core-excited transitions were observed. The width obtained from a Gaussian fit (dashed curve in Fig. 5) to the experimental longitudinal momentum distribution is 59 ± 3 MeV/c (after correcting for the experimental resolution). This width is larger than the value of 48 ± 3 MeV/c measured by Bazin *et al.* [8] for Coulomb breakup on a tantalum target at 86 MeV/nucleon. However, it agrees within the errors with that extracted from the ^{13}B ground-state longitudinal momentum distribution for the Be target in the present work. The integrated cross section derived for Coulomb breakup of ^{14}B on ^{197}Au (leaving the ^{13}B core fragment in the ground state) is 638 ± 45 mb, much larger than the yield quoted in Ref. [8]. It was suggested there that the

smaller cross section reflected a quenching of the soft dipole strength that implied ''normal'' nuclear structure for ^{14}B. However, a possible experimental problem due to the restricted angular acceptance of the A1200 spectrometer was acknowledged. The present observations of a broader momentum distribution coupled with a larger cross section suggest that this was indeed the case.

The Coulomb breakup cross section was calculated using a Yukawa potential with finite-size corrections [21]. The result, 543 mb, is less than our measurement. However, the yield calculated in Ref. [8] using a Woods-Saxon potential was 50% larger than that from the Yukawa form. Our data suggest that the actual situation is intermediate between these two approximations. The Coulomb contribution to our Be-target data was also computed and found to be negligibly small (2.3 mb). The solid curve in Fig. 5 shows the longitudinal momentum distribution for the Au target predicted in the model of Ref. [21], normalized to the experimental data. The width of this Lorentzian function compares well with experiment, but the agreement in the tails of the distribution is unsatisfactory.

D. Neutron halo in ^{14}B

Zhongzhou *et al.* [22] have predicted an inversion of the $1d_{5/2}$ and $2s_{1/2}$ orbitals for ^{14}B within the framework of a nonlinear relativistic mean-field calculation. Their calculation shows that, under these conditions, ^{14}B is a neutron halo nucleus. This is in agreement with the shell-model calculation cited above and with our observation of a dominant $l=0$ component in the ground state of this nucleus. The width of the corresponding longitudinal momentum distribution (55 ± 2 MeV/c) is a factor of 2.5 smaller than that of the core-excited states and only slightly larger than the value (45.7 ± 0.6 MeV/c) measured [3] for the well-known halo nucleus ^{11}Be. This implies strong spatial delocalization of the valence neutron orbital. An illustration of this effect can be seen in Fig. 2 of Ref. [8].

Measurements of the interaction cross sections at relativistic energies for particle-stable B isotopes ranging from mass 8–15, by Tanihata *et al.* [23], suggested that their effective rms radii are practically constant, which does not support the halo hypothesis. However, measurements at intermediate energy, analyzed by Liatard *et al.* [24], gave larger rms radii in all cases than those of Ref. [23], together with a significant mass dependence and an anomalously large radius for ^{14}B. The radius difference is not by any means as large as in the case of ^{11}Li, for example, but this is not unexpected given the fact that the valence neutron is more tightly bound in ^{14}B. Of course, the rms radius extracted from an interaction cross section is not the only signature for halo structure [25–27], and the narrow longitudinal momentum distribution and large cross section for dissociation of the ground state of ^{14}B observed in the present experiment strongly argue for halo structure in this system.

IV. SUMMARY

In this experiment, we have measured the longitudinal momentum of the ^{13}B core fragment in one-neutron knockout from ^{14}B, on both ^{9}Be and ^{197}Au targets. The contribution from core excitation was isolated by measuring the excited ^{13}B fragments in coincidence with γ rays from their decay. Comparison of the observed intensities of core-excited γ-ray transitions with a shell-model calculation, using an eikonal reaction theory, allowed us to make spin assignments for two positive-parity excited states in ^{13}B. The longitudinal momentum distributions in coincidence with the positive-parity core-excited transitions are consistent with knockout from a $1p_{1/2}$ state, as expected. An excellent fit to the distribution obtained when the ^{13}B core remains in its ground state is also provided by the shell-model calculation, which predicts an admixture of $2s_{1/2}$ and $1d_{5/2}$ neutron knockout. The experimental data imply an $89\pm3\%$ $l=0$ component, in agreement with the shell-model result. The Coulomb breakup cross section, measured with the ^{197}Au target, is consistent with expectations for a weakly bound $2s_{1/2}$ neutron. The width of the longitudinal momentum distribution obtained with the ^{197}Au target (59 ± 3 MeV/c) agrees with that obtained using the ^{9}Be target after the core-excited component is subtracted.

The results of the present experiment lend very strong support to the idea that ^{14}B is a ''neutron-halo'' system, the first odd-odd nucleus to display this structure. It also appears that, with the sole exception [8] of ^{17}C at $N=11$, all of the lowest-mass, particle-stable isotones from $N=7-13$ are halo nuclei. It therefore seems that reinvestigation of the structure of ^{17}C is in order.

ACKNOWLEDGMENTS

The first author (V.G.) was financially supported by FAPESP (Fundação de Amparo a Pesquisa do Estado de São Paulo–Brazil) while on leave from the UNIP (Universidade Paulista). This work was supported by the National Science Foundation under Grant Nos. PHY94-02761, PHY99-01133, PHY95-14157, and PHY96-05207.

[1] P. G. Hansen, A. S. Jensen, and B. Jonson, Annu. Rev. Nucl. Part. Sci. **45**, 591 (1995).
[2] A. Navin *et al.*, Phys. Rev. Lett. **81**, 5089 (1998).
[3] T. Aumann *et al.*, Phys. Rev. Lett. **84**, 35 (2000).
[4] V. Maddalena *et al.* (unpublished).
[5] M. H. Smedberg and M. V. Zhukov, Phys. Rev. C **59**, 2048 (1999), and references therein.
[6] T. Nakamura *et al.*, Phys. Rev. Lett. **83**, 1112 (1999).
[7] T. Baumann *et al.*, Phys. Lett. B **439**, 256 (1998).
[8] D. Bazin *et al.*, Phys. Rev. C **57**, 2156 (1998).
[9] B. M. Sherrill, D. J. Morrissey, J. A. Nolen, Jr., and J. A. Winger, Nucl. Instrum. Methods Phys. Res. B **56&57**, 1106 (1991).
[10] H. Scheit *et al.*, Nucl. Instrum. Methods Phys. Res. A **422**, 124 (1999).
[11] B. M. Sherrill (unpublished); J. A. Caggiano, Ph.D. thesis,

Michigan State University, 1998; J. Yurkon, D. Bazin, W. Benenson, D. J. Morrissey, B. M. Sherrill, D. Swan, and R. Swanson, Nucl. Instrum. Methods Phys. Res. A **422**, 291 (1999).
[12] GEANT, CERN Library Long Writeup W5013, 1994.
[13] F. Ajzenberg-Selove, Nucl. Phys. **A523**, 1 (1991).
[14] E. K. Warburton, B. A. Brown, and D. J. Millener, Phys. Lett. B **293**, 7 (1992).
[15] E. K. Warburton and B. A. Brown, Phys. Rev. C **46**, 923 (1992).
[16] F. Ajzenberg-Selove, E. R. Flynn, and O. Hansen, Phys. Rev. C **17**, 1283 (1978).
[17] J. A. Tostevin, J. Phys. G **25**, 735 (1999).
[18] M. Berz *et al.*, Phys. Rev. C **47**, 537 (1993).
[19] N. A. Orr, Phys. Rev. C **51**, 3116 (1995).
[20] P. G. Hansen, Phys. Rev. Lett. **77**, 1016 (1996).
[21] R. Anne *et al.*, Nucl. Phys. **A575**, 125 (1994).
[22] Zhongzhou Ren *et al.*, Z. Phys. A **357**, 137 (1997).
[23] I. Tanihata *et al.*, Phys. Lett. B **206**, 592 (1988).
[24] E. Liatard *et al.*, Europhys. Lett. **13**, 401 (1990).
[25] N. A. Orr, Nucl. Phys. **A616**, 155c (1997).
[26] K. Riisager, Nucl. Phys. **A616**, 169c (1997).
[27] V. Guimarães *et al.*, Phys. Rev. Lett. **84**, 1862 (2000).